Characterization of 3D printed long fibre reinforced composites

J. Justo, L. Távara*, L. García-Guzmán, F. París

Grupo de Elasticidad y Resistencia de Materiales,
Escuela Técnica Superior de Ingeniería, Universidad de Sevilla,
Camino de los Descubrimientos s/n, 41092 Sevilla, Spain

Abstract

Additive Layer Manufacturing (ALM) process is used in the present investigation to manufacture long fibre reinforced composite parts using the MarkOne® 3D-printer. In ALM, a continuous filament (including a tow of fibres) of composite material is injected by the printer, at high temperature, over a plain tool, forming the part while the material is cooled down. The used composite filament is formed by a PA (Nylon™) matrix and carbon or glass fibre reinforcements. Previous works have shown an improvement on the mechanical properties of a part, when some zones include a nylon based composite reinforcement using ALM. Nevertheless, the characterization of fully made nylon-based ALM composite material parts has not been reported. Thus, the aim of this investigation is the experimental characterization of composite nylon-based coupons. The plane strength and stiffness properties of the composites are obtained, both for tensile and compression load states. Results showed that the obtained mechanical properties for ALM composites are not yet comparable to those obtained by traditional methods (pre-pregs). This fact may be explained by the high porosity found in ALM coupons as well as a low fibre volume obtained. Nevertheless, the mechanical properties improvement in comparison to non-reinforced nylon parts

*Corresponding author. Tel.:+34 954487299; Fax: +34 954461637
Email address: ltavara@us.es (L. García-Guzmán)

is remarkable.

Keywords: ALM, FDM, long fibre composites, mechanical characterization

1. Introduction

The large number of complex processes involved in the manufacturing of composite materials regarding the traditional manufacturing techniques entail long production times and elevated costs. Furthermore, these techniques, due to the kind of raw materials used, imply the generation of scraps. New processes are explored to circumvent these problems. The very best way to do, it is to implement and automate all the steps in a single process. One alternative is the use of Additive Layer Manufacturing (ALM), usually named 3D printing, in which the material is laid up, compacted and cured at the same time. On the way the material is laid-up, it is cooled and solidified, achieving 3D geometries without using complex moulds. ALM technologies are experiencing an important rise in the production of aeronautical parts. In the past, its use has been dedicated to very low structural responsibility parts. In the last decade, there has been an increasing interest in introducing these technologies in the manufacturing of structural parts [1, 2]. In fact, the use of ALM technologies in nanostructures was also studied, see [3]. Some of the advantages of ALM technologies compared to the traditional manufacturing procedures are: (i) the manufacturing of the parts does not require the use of moulds; (ii) there are almost no scraps after manufacturing; (iii) the manufactured parts require less post treatments(or even nothing); (iv) after the design of the part, all the process is automated,avoiding human mistakes.

Two kinds of materials are mostly used in ALM processes: metallics and plastics. The metallic materials offer high mechanical properties, capable to compete with metallic parts manufactured by casting or machining [4]. In the case of the plastic parts, its properties are very poor and they are not capable to directly substitute other materials for structural parts. In order to improve the

properties of these parts, the introduction of fibre reinforcements was studied by several authors.

A review on different ALM techniques, applications and actual needs can be found in [5, 6, 7, 8], while different techniques, specifically for fibre reinforced plastics, are summarized in [2, 9, 10, 11, 12]. The evolution on composites may start with one of the first attempts to improve the mechanical properties of 3D printed polymers (including continuous glass fibres and a photopolymer) presented in [13]. The technique used was 3D photolithography, able to include around a 6% of fibre volume. Later on, using the same technique, carbon fibres were included and also the fibre volume was increased to approximately 30% in [14]. The effect of a dual (photo and thermal) curing for carbon reinforced photo polymer is studied in [15]. Glass (short) fibres were also used to reinforce a photopolymer in [16, 17]. Moreover, a comprehensive study on the obtained mechanical properties using this kind of reinforcement can be found in [18, 19].

Another ALM technique used to manufacture polymer composites is the so-called Laminated Object Manufacturing (LOM). In [20], LOM is used with glass fibre/epoxy matrix pre-pregs, a study on the different interfaces appearing in the composite being also included in that investigation.

Nowadays, the Fused Deposition Modelling (FDM) is the ALM plastic technology considered adequate to combine the fibre reinforcements and a polymeric matrix. In the FDM technology, a thermoplastic filament is extruded through an injector, heated to the fusion temperature of the plastic, and placed over a plain mould. As the material is cooled down once placed, it turns into a solid and reaches its final shape. The final 3D geometries are manufactured from 2D layers [21].

For the FDM case, several possibilities for introducing the filament into the plastic have been considered [22, 23]:

(i) Embbeding the fibre directly in the component: In this case, two injectors

are needed, one for the resin and another for the fibre. The fibre and the matrix are mixed at the part, once injected.

(ii) Embedding the fibre in the injector: In this case, the fibre and the resin are mixed in the injector, just before the injection process.

(iii) Embedding the fibre previously to the injection: In this case, a pre-impregnated filament containing both the fibre and the resin is used. It is interesting to notice that this kind of filament can be used in a traditional FDM machine, just with a modification of the injectors.

It is noticeable that FDM on composites has several common characteristics to well-established procedures as automated fibre placement [24] and filament winding. The latter has been used with carbon, glass and Kevlar fibres pre-impregnated with thermoplastic resins such as PEEK and polypropylene [25, 26, 27]. The main difference between those procedures and FDM, is that FDM does not need the use of a mould which follows the final shape of the part, as support columns (if needed) can be printed together with the desired part.

In [28], carbon fibre is included in ABS using a FDM technique, while PLA is used in [29, 30]. Mechanical tests were performed to characterize the obtained composites. Finally, the effect of including glass fibres on some zones of nylon (NYL-AB-1K supplied by MarkForged®, Somerville, MA) coupons is studied in [31].

In the present investigation, fully reinforced coupons made of glass and carbon fibre filaments (supplied by MarkForged®, Somerville, MA), manufactured using FDM, will be characterized. The filaments include a tow of fibres which are embedded (previously to the injection) in nylon. First, some details of the 3D commercial printer MarkOne® [32] and the mechanical tests carried out are presented. Then, the results of the characterization tests are discussed.

2. Printer description

A MarkOne® 3D printer, manufactured by Markforged [32] has been the ALM/FDM system used in the present investigation. A picture of the printer can be seen in Figure 1(a). The system can print two kind of materials independently and, for this reason, it has two extruders and two injectors, see Figure 1(b). One of the injectors is used to print nylon (as the traditional 3D plastic printers can do) and the other one is used to print fibre reinforced thermoplastics. The nylon injector can be also used, in addition to print parts, to print supports when needed. The supports are material plies used to hold the printing in zones of the parts that have a cantilever configuration. Once the part is manufactured, the supports are discarded.

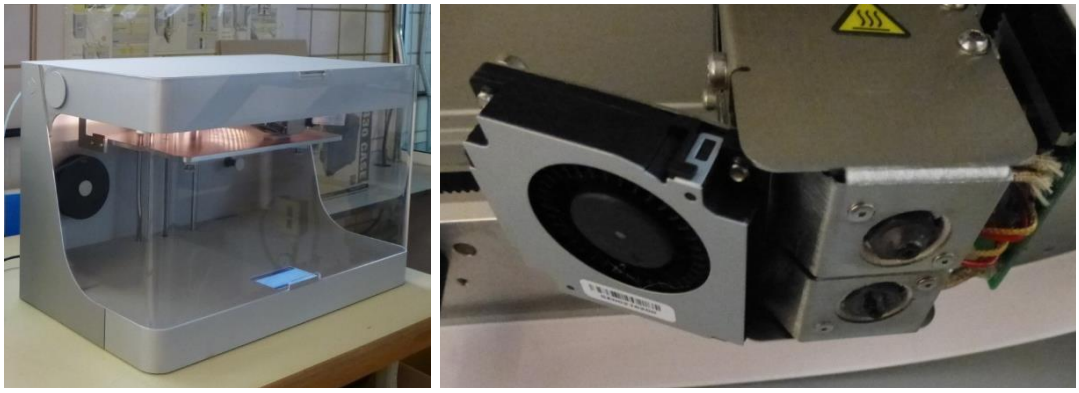

(a) (b)

Figure 1: (a) General view of the 3D printer. (b) Detail view of the two printer injectors.

MarkOne® was considered as the first printer able to print composite parts. It was released by the end of 2014. Later, on February 2016 MarkTwo® printer was released and MarkOne® was discontinued. Nevertheless, both printers share similar technical characteristics. It should also be mentioned that updates are available for every printer model. MarkOne® uses its own software called Eigen®. 3rd party software cannot be used with the printer but the software allows to import .STL and .OBJ models. The orientation of the fibres can be controlled

through the software. It allows to specify the fibre orientation on a layer-by-layer basis. The build size allows to print parts with the maximum following dimensions 320 mm x 132 mm x 160 mm.

MarkOne® printer is able to manufacture carbon, glass and arimidic (Kevlar™) fibre reinforced nylon parts. The used filaments are supplied by Markforged. These filaments consist on a mixture of a bundle of long fibres and resin, forming a preimpregnated-like material. A view of the glass fibre/nylon and carbon fibre/nylon filaments is shown in figure 2. The same filaments, after a calcination (where the resin has been removed), are also shown in the figure. Notice that the bundle of fibres can be clearly observed once the calcination is done. The aim of the calcination was to check the amount of fibres and resin present in the filament. Results showed an approximated 40% fibre weight for the carbon fibre filament and almost a 50% for the glass fibre case. Fibre volume fractions will be presented once the micrographs of the printed material are studied in the Discussion Section. In the following, the way the printer works with the fibre reinforced filament is described:

- The injector is heated up to the fusion temperature of the matrix.
- The fibre reinforcement filament is pushed through the injector.
- The resin is fused and the composite is placed over the printing bed, following a programmed pattern.
- The resin is cooled down just after having been laid up, obtaining the composite's final shape.
- Once the whole layer has been laid-up, the printing bed is moved down, allowing a new layer to be printed.

When printing nylon or glass fibre reinforced nylon, the geometry can be obtained following several printing patterns (rectangular and circular) making

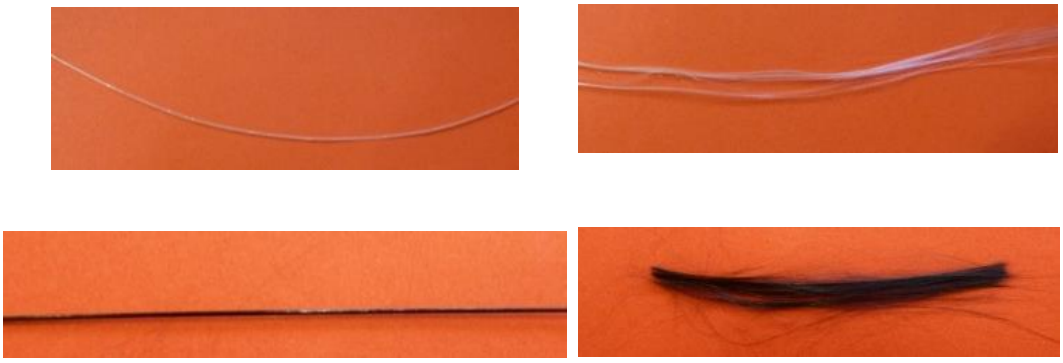

(a) (b)

Figure 2: Glass and carbon fibre filaments (a) before and (b) after calcination.

it possible to give orientations to the fibre in each layer (using the rectangular pattern). In the case of the carbon fibre reinforced nylon, due to the stiffness of the fibre, to print following a circular pattern is only allowed.

Notice that the printing system only allows the reinforcement to be placed in the plane of the parts. Thus, it is a 2.5D printing system, as usual in all the ALM systems that can be found in the market nowadays.

It is important to notice that, during the printing procedure, no pressure is applied after a layer is laid up. It is well known that pressure plays a fundamental role on the manufacturing of laminated parts for both thermoset and thermoplastic based composites. The absence of pressure in highly viscous matrices is directly related to the presence of large defects (pores and matrix-dominated zones). Moreover, the use of an injector during the printing procedure may lead to some waviness effect on the fibres. Both aspects will be studied on the Discussion section.

3. Tests and coupons description

The characterization of the in-plane material properties was done by means of tensile and compression tests, following the corresponding standards. In-plane shear properties, obtained using a $\pm 45^{\circ}$ laminate, were only obtained for the glass

fibre. As stated before, the way the carbon fibre reinforced nylon is allowed to be printed (following closed elliptical patterns in a plane, see figures 3(a) and 3(b)) difficults a ±45° carbon laminate to be manufactured. The tests done and their corresponding coupons are described in the following.

3.1. Tensile test

The tests were carried out following ASTM D3039 standard [33], to characterize both glass fibre and carbon fibre composites in the direction of the fibres. The glass fibre coupons were printed one at a time. In the case of the carbon fibre coupons in the direction of the fibres, they were obtained manufacturing a panel, as the one shown in figure 3(c), and cutting them later on.

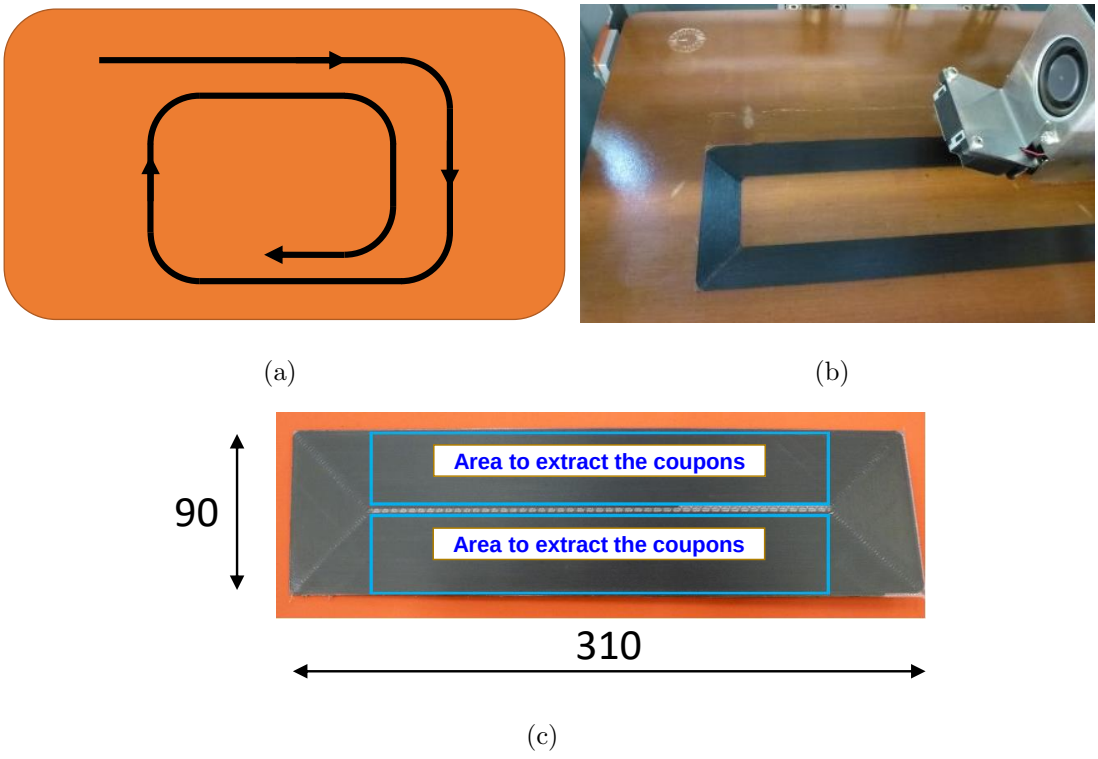

Figure 3: (a) Schme of the carbon fibre composite printing process.(b) Carbon fibre composite printing process. (c) Zones of the carbon fibre panel used to extract the coupons, dimensions included are in mm.

Glass fibre and carbon fibre tensile test coupons in the direction of the fibre

were manufactured with the following dimensions: height 250 mm, width 12.5 mm and thickness 1 mm. For the glass fibre, also tensile tests were carried out in the direction perpendicular to the fibres. Coupons dimensions are height 175 mm, width 25 mm and thickness 2 mm. In the case of carbon fibre composites, tensile properties perpendicular to the fibre were not obtained, due to the impossibility to obtain this kind of coupons due to the printing process of carbon fibres already commented.

According to the standard, the coupons must include some tabs at their ending zones in order to avoid any damage that many be produced by the gripping system. Thus, for the case of the glass fibre, the coupons tabs were initially thought to be printed at the same time of the coupons (following a $\pm 45^{\circ}$ stacking sequence). It is important to remark that, in order to include the space between the printing bed and the coupon itself (a cantilever configuration appears due to the presence of the tabs) support material was added during the manufacturing and then removed. Nevertheless, it was seen that this way of printing was inefficient, requiring long printing times and lots of material just for obtaining the tabs. Finally, $\pm 45^{\circ}$ pre-preg glass fibre tabs were manufactured (in a traditional way) and bonded to the coupons.

3.2. Compression test

The tests were carried out following ASTM D695-02a standard [34]. The tests were done both in the direction of the fibres and in the direction perpendicular to the fibres. Note that, following the standard, two different sets of coupons had to be manufactured and tested for each type of material, one for the determination of the elastic modulus and one for the determination of the strength. Coupons dimensions (being the same for both sets) are height 80 mm, width 12.5 mm and thickness 2 mm. The only difference is that modulus coupons does not need the use of tabs. As in the previous case, glass fibre coupons were obtained printing them individually and the carbon fibre ones were obtained from a panel.

It should be remarked that the compression fixtures used (according to the standard) requires a minimum coupon length. Then, due to the limitations (on size) of the printer, carbon fibre coupons oriented perpendicular to the fibre required an added supplement, with height 14 mm. The supplement is added in one of the extremes of the coupon, in order to get to the needed 80 mm in total height. Results presented in the Test results section showed that the use of the supplements do not affect the compression failure, as they are located far from the failure zone of the coupons.

3.3. In-plane shear test

The tests have been carried out following ASTM D3518 standard [35]. Due to the stacking sequence required by these coupons and the way the equipment prints the different filaments, the test has only been carried out for the glass fibre case. As stated before, it is not possible to print $\pm 45^{\circ}$ laminates with the carbon fibre filament. These coupons were printed individually with the following coupons dimensions: height 175 mm, width 20 mm and thickness 2 mm.

3.4. Microscopic observation

Several coupons were inspected with an optical microscope, with the purpose to observe the internal structure of the material after the manufacturing process. As stated previously, the absence of pressure during the printing may lead to a large number of defects. Typical preparation for the microscope inspection was done including: coupons cut, embed in resin and polish. The results of the observations will be presented in the Discussion section. The image treatment software Perfect Image® from Clara Vision™ has been used to treat the obtained pictures.

4. Test results

The results of the mechanical tests are presented separately for each material. For the sake of clarity, three stress/strain curves and a picture of a broken

coupon are presented for each type of test. It should also be mentioned that the curves that will be shown are those obtained using the moving crosshead of the testing universal machine and they are used to get the strength parameters. Nevertheless, an extensometer or strain gauges (for tensile and compressive coupons respectively) were also used during the initial stage of the tests. The curves obtained with the extensometer/strain gauge are not presented herein as they just shown the initial stage of the test, but they were used to obtain the stiffness parameters.

4.1. Test results for the carbon fibre reinforced coupons

4.1.1. Tensile test in the direction of the fibres

The obtained load-displacement curves for the tensile test can be seen in figure 4(a). After an initial adjustment between the gripping system and the coupons, a linear evolution can be appreciated until reaching the failure load. For coupons of this kind, an explosive failure could be expected, due to the alignment of the fibre with the load. Neverthelesss, as can be seen in figure 4(b), the failure has occurred with a break almost perpendicular to the loading direction. This fact occurred in all coupons of the set and it may be explained by the presence of internal defects in the coupons. Defects that can be found in printed parts will be described in the Discussion section.

4.1.2. Compression test in the direction of the fibres

The load-displacement curve for the compression test can be seen in figure 5(a). It should be noticed that the test curves used to obtain the modulus are not shown, for the sake of brevity. Moreover, the load values have turned positive, in order to make the curves easier to read. Again, after an initial adjustment between the compression fixture and the coupons, the apparent stiffness grows until achieving a constant and a linear evolution of the curve to failure. The steps (jumps) that can be appreciated in the curves are caused by the small values of

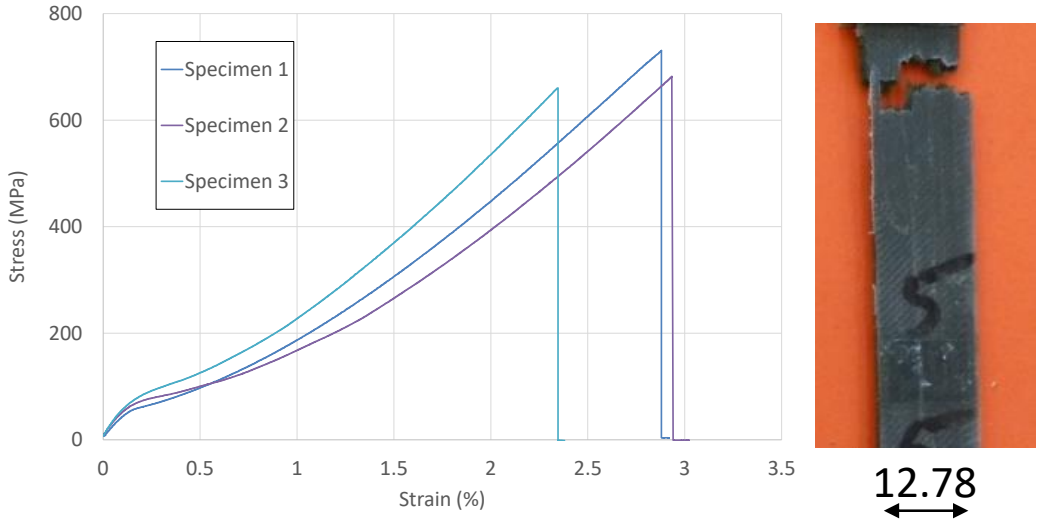

(a) (b)

Figure 4: (a) Carbon fibre load-displacement curves of the tensile test in the direction of the fibres and (b) detail of the failure of a coupon. The characteristic dimension is in mm.

the applied displacement, showing the increments the machine applies. Failure occurs in the free zone between the tabs (see figure 5(b)) and at an angle of $35° \pm 5°$ (following a V-shape evolution) measured from the longitudinal direction (figure 5(c)).

4.1.3. Compression test in the direction perpendicular to the fibres

The load-displacement curve corresponding to this test can be seen in figure 6(a). Once again the curves of the tests used to obtain the modulus are not shown and the load values have turned positive. The tests starts with an initial adjustment between the compression fixture and the coupons. Then, the apparent stiffness increases until achieving a constant value and the curve follows a linear evolution until reaching its maximum load. Finally, the stiffness decreases until reaching a plateau, that may be attributed to plastic effects in the matrix (that smooths the evolution of the curves during the failure). Failure occurs in the free zone between the tabs (see figure 6(b)) and at an angle of $25° \pm 7°$, measured

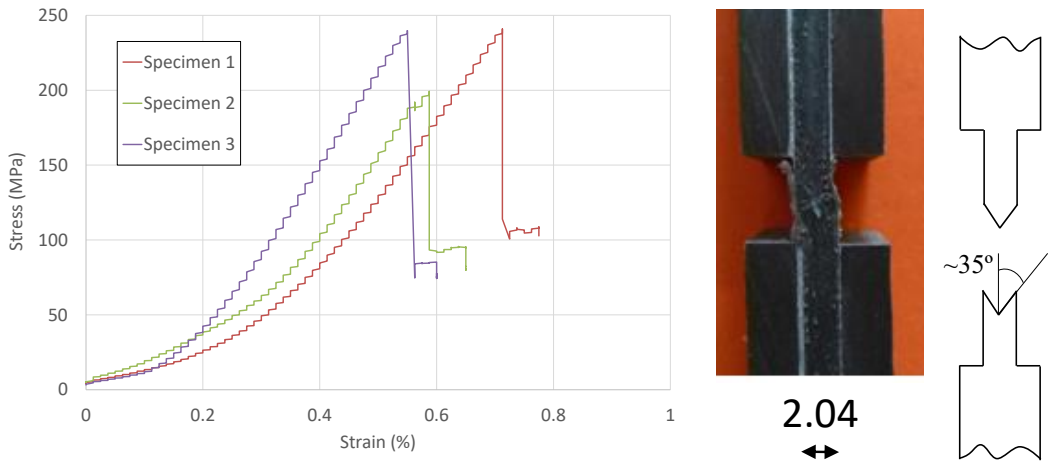

(a) (b) (c)

Figure 5: (a)Carbon fibre load-displacement curves of the compression test in the direction of the fibres, (b) detail of the failure of a coupon, the characteristic dimension is in mm and (c) scheme of the failure angle.

from the longitudinal direction (figure 6(c)).

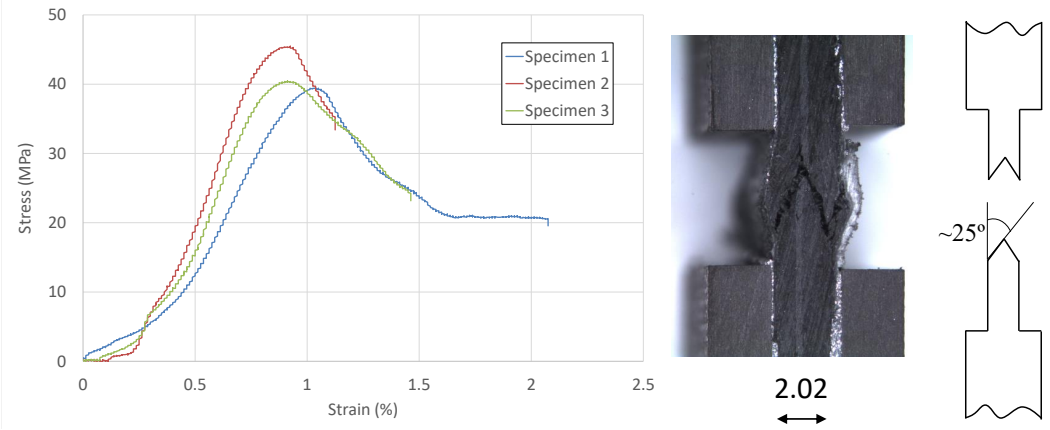

(a) (b) (c)

Figure 6: (a) Carbon fibre load-displacement curves of the compression test in the direction perpendicular to the fibres, (b) detail of the failure of a coupon, the characteristic dimension is in mm and (c) scheme of the failure angle.

4.2. Test results for the glass fibre reinforced coupons

4.2.1. Tensile test in the direction of the fibres

The load-displacement curves are plotted in figure 7(a). A linear evolution can be seen until reaching the failure load. The failure mechanisms were different for both carbon and glass 0° coupon sets. In glass, failure appeared at several places of the specimens (at the center and close to the tabs) perpendicular to the load, generating cracks in the direction parallel to the fibres 7(b). This type of failure is usually known as "green wood failure mode [36].

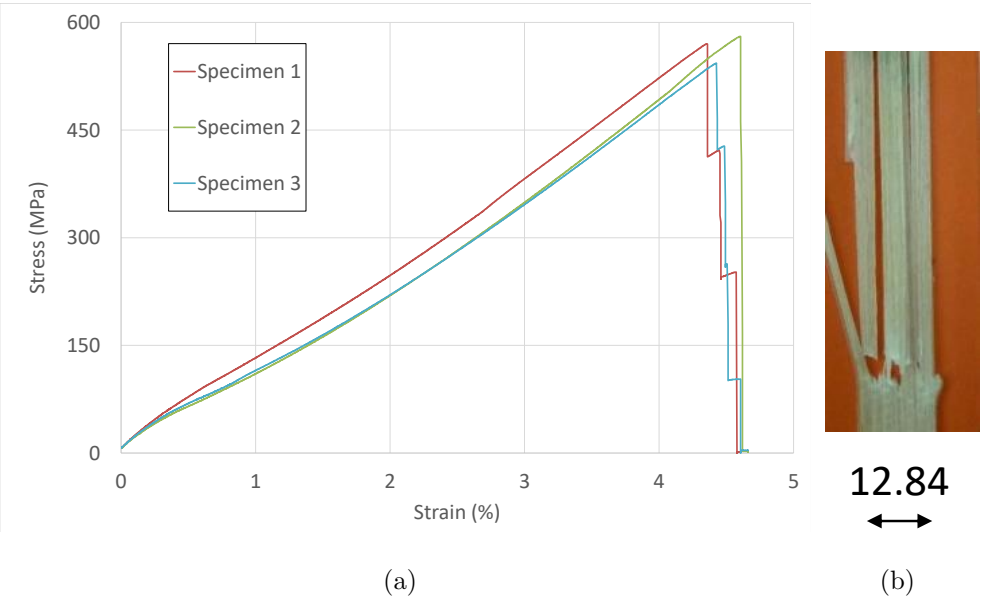

(a) (b)

Figure 7: (a) Glass fibre load-displacement curves of the tensile test in the direction of the fibres and (b) detail of the failure of a coupon. The characteristic dimension is in mm.

4.2.2. Compression test in the direction of the fibres

Load-displacement curves are presented in figure 8(a). As for the case of the carbon fibre, the curves of the tests made to obtain the modulus are not plotted and the load values have turned positive. A linear evolution can be seen until reaching the failure load. As in the case of carbon fibre coupons, steps can be observed in the curves due to the way the displacement increments are applied.

Failure occurs in the free zone between the tabs (see figure 8(b)) and at an angle of $35° \pm 5°$, following a V-shape, measured from the longitudinal direction (figure 8(c)).

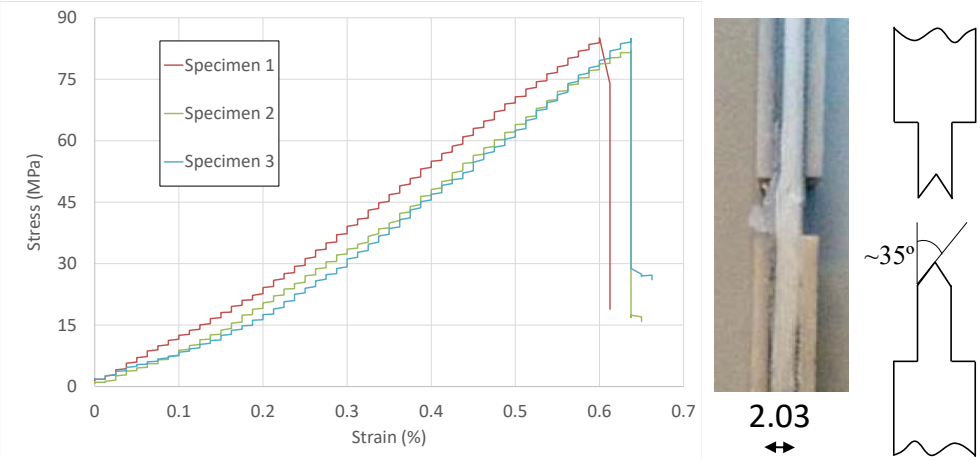

(a) (b) (c)

Figure 8: (a) Glass fibre load-displacement curves of the compression test in the direction of the fibres, (b) detail of the failure of a coupon, the characteristic dimension is in mm and (c) scheme of the failure angle.

4.2.3. Tensile test in the direction perpendicular to the fibres

The load-displacement curve for the tensile test can be seen in figure 9(a). A linear evolution can be seen at the beginning of the curves, until reaching a 25% of the final load approximately. Then, due to plastic effects related to the matrix, a non-linear evolution can be observed until reaching the final load. The failure, as expected, occurred at a plane parallel to the fibres and perpendicular to the load (see figure 9(b)).

4.2.4. Compression test in the direction perpendicular to the fibres

The load-displacement curves for the compression test are presented in figure 10(a). A non-linear evolution until failure can be appreciated during the tests, because of the role that the matrix plays in this case. The failure has occurred

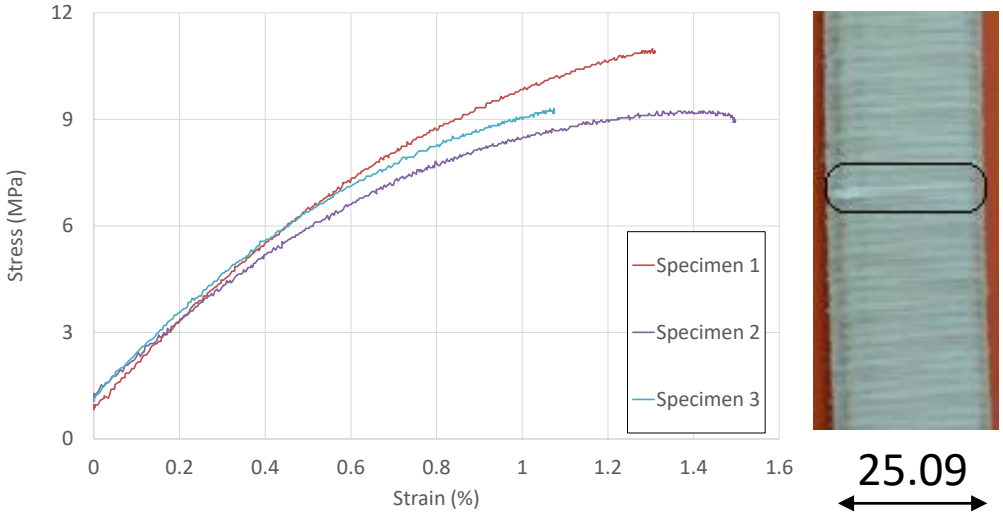

(a) (b)

Figure 9: (a) Glass fibre load-displacement curves of the tensile test in the direction perpendicular to the fibres and (b) detail of the failure of a coupon. The characteristic dimension is in mm.

at a line perpendicular to the load (figure 10(b)), producing a posterior lateral deviation and the buckling of the free zone of the coupons. It is noticeable the differences on the fracture surface, with respect of those for the carbon fibre (figure 6(b)). These differences could be motivated by several aspects. One of them may be the way the coupons were printed. The carbon fibre coupons were cut from a panel, i.e. the fibres end at the borders of the coupon (see figure 11(a)). On the other hand, the glass fibre coupons were printed one by one, i.e. the fibres are continuous throughout the coupons (see figure 11(b)). Futhermore, independently of the different way of printing the carbon and glass specimens. It seems, looking at the broken specimens, that two different mechanisms of failure are involved in both cases. Thus, the failure mechanism of carbon specimen is controlled by the breakage of the fibre-matrix interface, see [37], giving rise to an apparent plane of failure. In this case an orientation of $\sim 25^\circ$ was obtained (see Figure 6). This result is in consonance with the numerical prediction obtained

based on the failure of the interface. On the contrary, in the case of glass specimen, the appearance of the failure is more connected to a local lateral instability of the specimen. Notice, to support these differences, that whereas in the case of carbon the maximum strain at failure is under 1%, in the case of glass specimens is clearly higher, in between 1 and 2%. This fact indicates that the failure in the case of carbon seems to be previous to the buckling of the coupon. In the case of glass, the measured strain may allow the local buckling of the coupon to be developed.

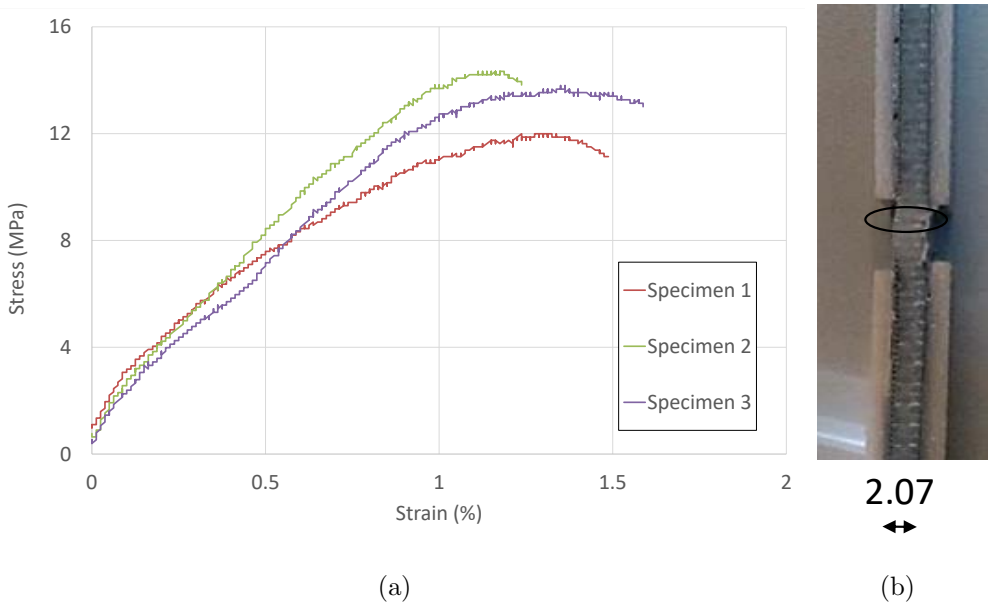

Figure 10: (a) Glass fibre load-displacement curves of the compression test in the direction perpendicular to the fibres and (b) detail of the failure of a coupon. The characteristic dimension is in mm.

4.2.5. In-plane shear test

The load-displacement curves for the in-plane shear are shown in figure 12(a). In this case, two different phases can be appreciated. At the beginning a convex curved evolution can be seen. It is motivated by the $\pm 45^{\circ}$ orientation of the fibres that tend to align to the load direction. This effect is usually referred to

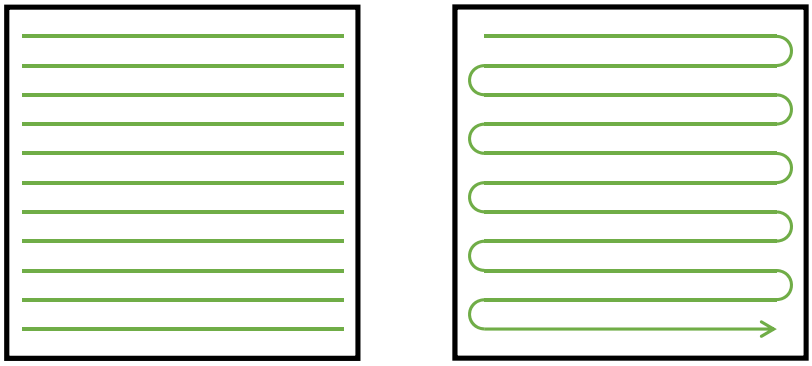

(a) (b)

Figure 11: Scheme of the fibres in the case of the (a) carbon fibre compression coupons and (b) glass fibre compression coupons in the direction perpendicular to the fibres.

as the scissor effect. Then, a concave curved evolution can be appreciated until reaching the final load. This effect is motivated by the tendency of the fibres to be pulled out of the matrix. Notice that this effect is also associated to large strain/displacements values during the test. The failure occurred following 45° lines, in which some fibres were pulled out and others broken (figure 12(b)). At this failure zone, the width decreased a 23% of the total coupon width, forming a neck on the coupon.

5. Discussion

The results of the mechanical tests are summarized in tables 1 and 2 for the carbon fibre and glass fibre composite, respectively, manufactured by ALM. Note that the scattering of the results is small, validating the obtained values. The smallest scattering can be found, as could be expected, in the tensile properties ruled by the behaviour of the fibres.

In order to study the possibility to use these materials in structural parts, the properties of the ALM composites have been compared with common pre-preg materials properties manufactured with vacumm bag and autoclave. The

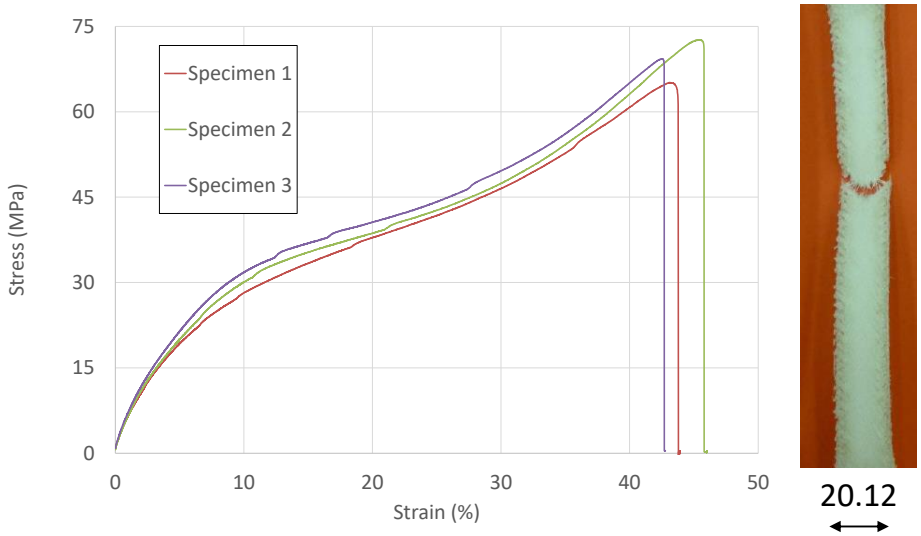

(a) (b)

Figure 12: (a) Glass fibre load-displacement curves of the in-plane shear test and (b) detail of the failure of a coupon. The characteristic dimension is in mm.

chosen materials are AS4 carbon fibre/epoxy composite and E-glass fibre/epoxy composite, with 69% and 65% fibre volume fraction, respectively. Pre-preg carbon composite properties were obtained in the laboratory using the previously mentioned standards (similarly to ALM composites), while pre-preg glass fibre composite properties are taken from literature [38]. The tensile and compressive properties of the carbon fibre materials and glass fibre materials in the direction of the fibres are shown in figures 13 and 14. The tensile properties of the glass

Test	**Property**	**Mean**	**Standard deviation**	**Covariance**	**Specific property**
Tensile 0°	X_T	701.41 MPa	70.00 MPa	9.98 %	588.43 kN m/Kg
	E_{11}	68.08 GPa	5.99 GPa	8.79 %	57.11 MN m/Kg
	ν_{12}	0.35	0.03	9.40 %	-
Compression 0°	X_C	223.06 MPa	29.92 MPa	13.41 %	187.14 kN m/Kg
	E_{11c}	52.99 GPa	0.97 GPa	1.83 %	44.45 MN m/Kg
Compression 90°	Y_C	41.83 MPa	3.20 MPa	7.65 %	35.09 kN m/Kg

Table 1: 40% fibre volume fraction ALM carbon fibre composite mechanical properties. Density of the carbon fibre laminate is 1192 kg/m^3.

Test	Property	Mean	Standard deviation	Covariance	Specific property
Tensile 0°	X_T	574.58 MPa	35.67 MPa	6.21 %	406.35 kN m/Kg
	E_{11}	25.86 GPa	1.90 GPa	7.36 %	18.29 MN m/Kg
	ν_{12}	0.37	0.04	11.35 %	-
Compression 0°	X_C	82.00 MPa	3.18 MPa	3.88 %	57.99 kN m/Kg
	E_{11c}	19.49 GPa	1.43 GPa	7.31 %	13.78 MN m/Kg
Tensile 90°	Y_T	9.84 MPa	1.01 MPa	10.14 %	6.96 kN m/Kg
	E_{22}	1.13 GPa	0.09 GPa	8.12 %	0.80 MN m/Kg
Compression 90°	Y_C	12.73 MPa	1.23 MPa	9.64 %	9.00 kN m/Kg
Shear	S	67.77 MPa	7.70 MPa	11.36 %	47.93 kN m/Kg
	G_{12}	0.88 GPa	0.10 GPa	9.94 %	0.62 MN m/Kg

Table 2: 50% fibre volume fraction ALM glass fibre composite mechanical properties. Density of the glass fibre laminate is 1414 kg/m^3.

fibre materials in the direction perpendicular to the fibres are shown in figure 15. The compression properties of the carbon and glass fibre materials in the direction perpendicular to the fibres are shown in figure 16. Finally, the shear properties of the glass fibre materials are shown in figure 17. Note that this is a qualitative comparison, as the polymeric matrix and the fibres are different for ALM and pre-preg manufactured composites.

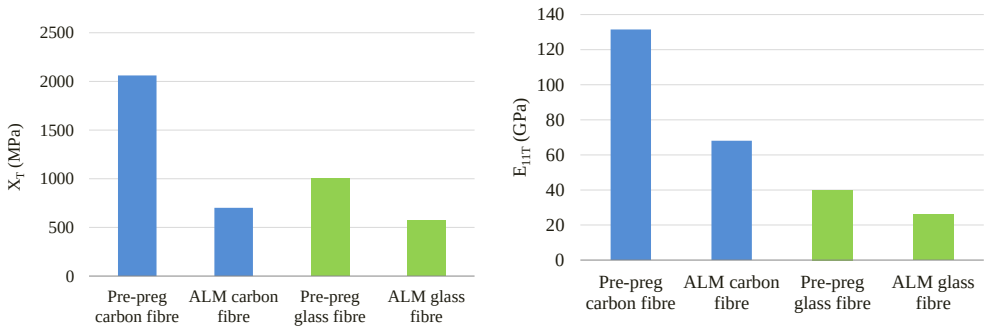

(a) (b)

Figure 13: Pre-preg vs ALM carbon fibre and glass fibre tensile properties in the direction of the fibres (a) X_T and (b) E_{11T}.

The comparison shows that the properties of ALM materials, compared with the pre-preg, are quite poor, both for the cases of the carbon and the glass fibres.

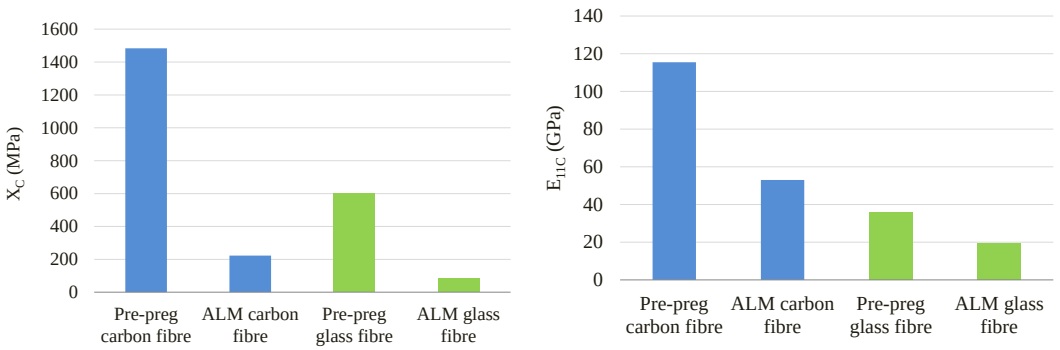

(a) (b)

Figure 14: Pre-preg vs ALM carbon fibre and glass fibre compression properties in the direction of the fibres (a) X_C and (b) E_{11C}.

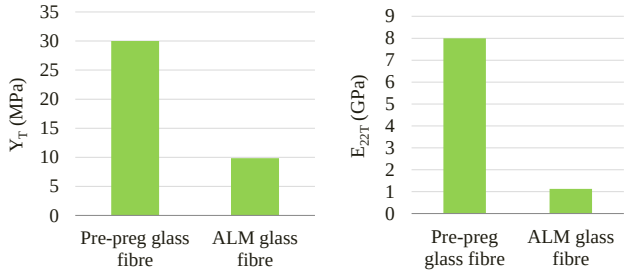

(a) (b)

Figure 15: Pre-preg vs ALM glass fibre tensile properties in the direction perpendicular to the fibres (a) Y_T and (b) E_{22T}.

The main causes of these differences are:

- The low properties of the raw materials of the ALM filaments and their low fibre volume fractions. Nylon has lower mechanical properties than the epoxy resin and the fibres used in ALM are low modulus and low strength fibres. The ALM parts have less fibres per volume than the prepreg materials (40% vs 69% in the carbon fibre and 50% vs 65% in the glass fibre). These are the main causes for the differences found in the tensile properties in the direction of the fibres and why the differences are higher in the case

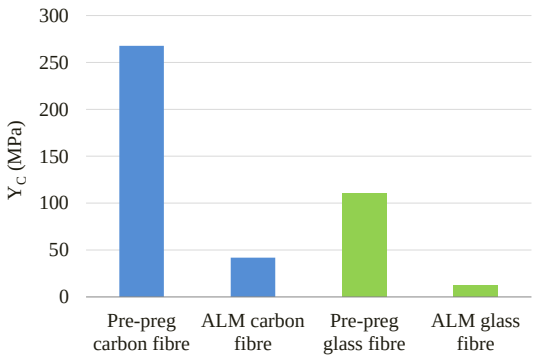

Figure 16: Pre-preg vs ALM carbon fibre and glass fibre compression properties in the direction perpendicular to the fibres, Y_C.

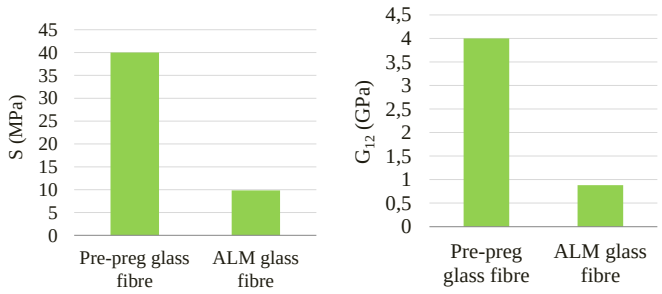

(a) (b)

Figure 17: Pre-preg vs ALM glass fibre shear properties (a) S and (b) G_{12}.

of the carbon fibre materials.

- The manufacturing process itself. As the layers of the material are manufactured filament by filament, without any compaction stage between filament laid up and even between layers, the final parts are very porous (∼12% and ∼17% for carbon and glass fibre composites, respectively). This fact can be observed in the micrographs shown in figure 18(a) and 18(b). The first micrograph corresponds to a carbon fibre panel and the second one to a glass fibre panel. On the figures, the black zones are the pores. It can also be seen that there are large matrix-dominated zones. These kind of defects

reduce the mechanical properties of the final parts.

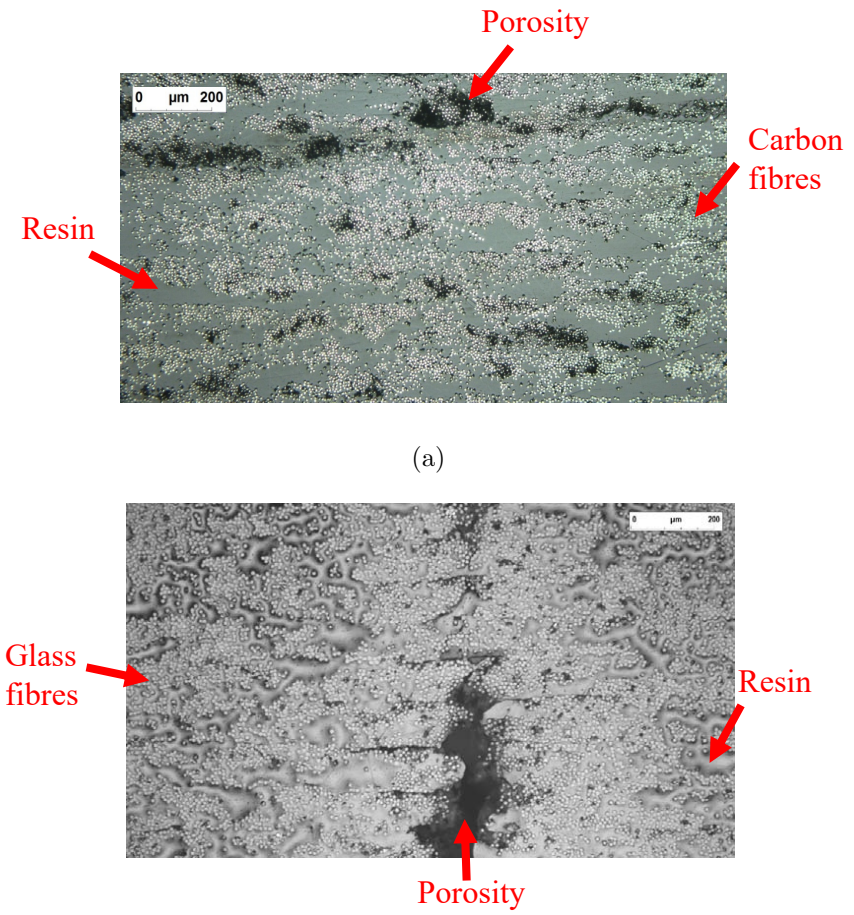

Figure 18: Micrographs of a laminate made of (a) carbon fibre/nylon composite and (b) glass fibre/nylon composite.

From the previous discussion, it is easier now to understand some results presented in Figure 13. For example, the differences between $E_{11T}^{cALM}/E_{11T}^{gALM} = 2.72$ and $E_{11T}^{cPP}/E_{11T}^{gPP} = 3.25$ can be explained by the differences in fibre volume ratio. Superscripts $cALM$ and $gALM$ stands for carbon and glass fibre composites manufactured by ALM, while cPP and gPP stands for carbon and glass fibre composites manufactured using prepregs.

It is interesting to notice, that although the use of an injector may lead to a large fibre undulation on the composite printed parts. The obtained fibre waviness is low. In order to see this effect, a picture of a glass fibre composite coupon which includes only one layer is presented. Figure 19 shows one of the most critical zone were waviness may appear, on the left it shows an edge of the coupon where the fibre tows turn back (see Figure 11(b) for a scheme). This picture shows that the printed fibre tows follows a parallel pattern, as they almost coincide with the auxiliary parallel lines plot on the picture for comparison purposes.

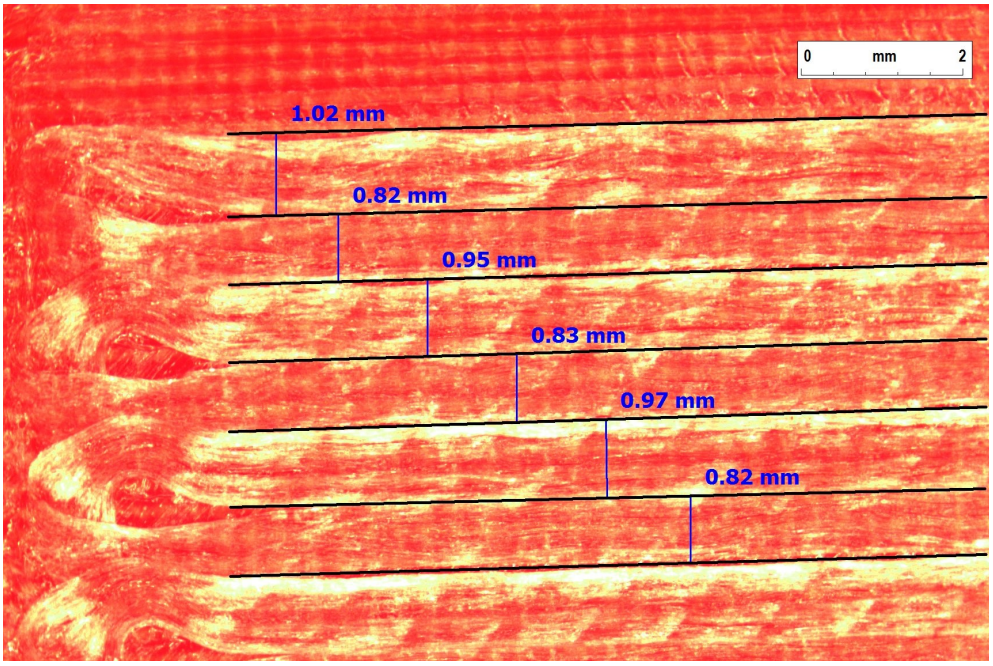

Figure 19: Micrograph of a glass fibre composite.

Another key feature on the printing process is the knowledge of the number of fibres within a filament. In figure 20, the micrographs for single printed filaments are shown. The measured carbon and glass fibre radius were around 3.4 μm and 4.7 μm, respectively. Then counting the number of the fibres on three different samples (for each type of filament) gives the following values: 960$\pm$50 and 374$\pm$10

for the carbon and glass fibre filaments respectively. Notice that in this pictures resin accumulation appears but porosity is very low. This fact leads to conclude that the high porosity ratio appears on the printed laminates as a consequence of an non-adequate joint between filaments (both side by side and layer by layer).

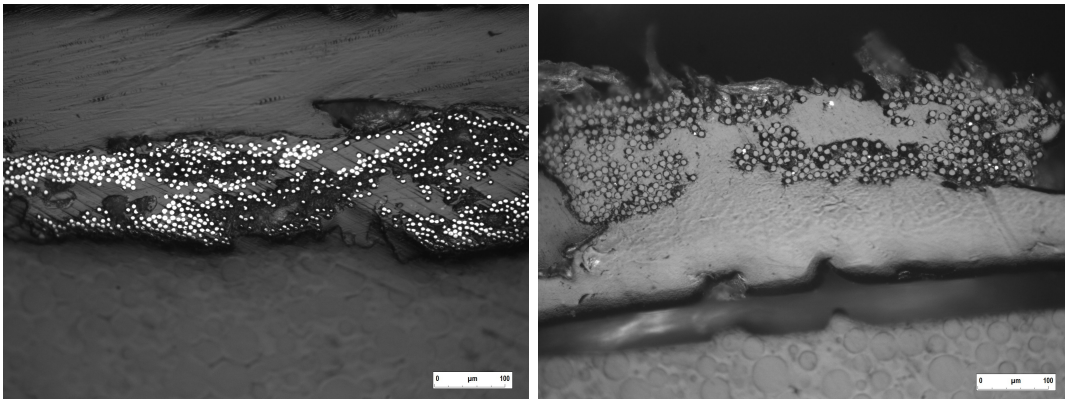

(a) (b)

Figure 20: Micrographs of a printed single filament made of (a) carbon fibre/nylon composite and (b) glass fibre/nylon composite.

In spite of the poor properties of the ALM material with respect to traditional pre-pregs, the reinforced ALM greatly improves the usual 3D printing parts. Thus, comparing the stiffness of the ALM glass fibre reinforced material (the one with the lowest mechanical properties) with the stiffness of a traditional 3D printing material (nylon), it can be seen that the properties of the ALM reinforced panels are much better. This effect can be observed in the direction of the fibres and also in the direction perpendicular to the fibres being E^{Nylon}=0.34 GPa, E_{22}^{Glass}=1.13 GPa and E_{11}^{Glass}=25.86 GPa. Morever, another advantage of the fibre reinforced 3D printing compared with the plastic printing is the stability that the fibre gives to the parts, reducing and even avoiding the shape distortions that usually appear in the printing of 3D parts [22].

In view of the obtained results, some ideas that will help in the improvement of the FDM composite mechanical properties are proposed:

- The use of a different resin (with better properties than nylon) as a matrix, for example PEEK.
- Produce a filament with a higher fibre content.
- Include a compaction stage after the deposition of the filaments, in order to diminish the pores content.

6. Conclusions

The mechanical characterization of long fibre reinforced plastics manufactured with an ALM machine has been carried out. Microscopic inspection of the materials was also done. The results showed that, at the present stage of the technology, the product obtained by ALM can not compete, in terms of mechanical properties, with the autoclave manufacturing of common pre-preg materials. One of the main reasons is that, independently of the raw materials supplied, the process does not allow to obtain an appropriate compaction of the material, generating porosity in the manufactured parts that decreases the final properties of the composites. Comparing this ALM materials with a usual 3D FDM plastic, the properties obtained are quite spectacular, due to the reinforcement of the fibres that multiplies the properties obtained several times. Thus, 3D FDM seems to be a very promising procedure to print long fibre composite parts once some of the current disadvantages are overcome.

The next steps of this work are the characterization of complex parts made with this technology and the study of a treatment to reduce the porosity in the parts, maybe including a compaction stage or reducing the viscosity of the material when printed.

Acknowledgements

This research was conducted with the support of the Spanish Ministry of Economy and Competitiveness (Projects MAT2015-71036-P and MAT2015-71309-P)

and the Junta de Andalucía and European Social Fund (Project of Excellence No. P12-TEP-1050).

References

[1] E., Klemp. Unterstützung des Konstrukteurs bei der Gestaltung von Spritzgussbauteilen Hergestellt im Rapid Prototyping und Rapid Tooling Verfahren (Support for Design of Injection Molded Parts Made by Rapid Prototyping and Rapid Tooling). Ph.D. thesis, Technische Universität Clausthal, 2002.

[2] X. Wang, M. Jiang, Z. Zhou, J. Gou, D. Hui. 3D printing of polymer matrix composites: A review and prospective. Composites Part B, 110 (2017) 442-458.

[3] O. Ivanova, C. Williams, T. Campbell. Additive manufacturing (AM) and nanotechnology: promises and challenges. Rapid Prototyping Journal, 19:5 (2013) 353-364.

[4] D.D. Gu, W. Meiners, K. Wissenbach, R, Poprawe. Laser additive manufacturing of metallic components: materials, processes and mechanisms, International Materials Reviews, 57:3 (2012), 133-164.

[5] N. Guo, M.C. Leu. Additive manufacturing: technology, applications and research needs. Frontiers of Mechanical Engineering, 8:2 (2013) 215-243.

[6] B.P. Conner, G.P. Manogharan, A.N. Martof, L.M. Rodomsky, C.M. Rodomsky, D.C. Jordan, J.W. Limperos. Making sense of 3-D printing: Creating a map of additive manufacturing products and services. Additive Manufacturing, 14 (2014) 64-76.

[7] D. Pollard, C. Ward, G. Herrmann, J. Etches. The manufacture of honeycomb cores using Fused Deposition Modeling. Advanced Manufacturing: Polymer & Composites Science, 3:1(2017) 21-31.

[8] J.M. Chacón, M.A. Caminero, E. García-Plaza, P.J. Nuñez. Additive manufacturing of PLA structures using fused deposition modelling: Effect of process parameters on mechanical properties and their optimal selection. Materials and Design, 124 (2017) 143-157.

[9] S. Kumar J.P. Kruth. Composites by rapid prototyping technology. Materials and Design, 31 (2010) 850-856.

[10] Z. Quan, A. Wu, M. Keefe, X. Qin, J. Yu, J. Suhr, J-H. Byun, B-S. Kim and T-W. Chou. Additive manufacturing of multidirectional preforms for composites: opportunities and challenges. Materials Today, 18:9 (2015) 503-512.

[11] A. Chiappone, I. Roppolo, E. Naretto, E. Fantino, F. Calignano, M. Sangermano, F. Pirri. Study of graphene oxide-based 3D printable composites: Effect of the in situ reduction. Composites Part B 124 (2017) 9-15.

[12] R.T.L. Ferreira, I.C. Ammatte, T.A. Dutra, D. Bürger. Experimental characterization and micrography of 3D printed PLA and PLA reinforced with short carbon fibers. Composites Part B 124 (2017) 88-100

[13] R. Charan, T. Renault, A.A. Ogale, A. Bagchi. Automated fiber-reinforced composite prototypes. Proc. Fifth Int. Conf. on Rapid Prototyping, June 1994, Dayton, Ohio, pp. 91-97.

[14] C. Greer, J. McLaurin, A.A. Ogale. Processing of carbon fiber reinforced composites by three dimensional photolithography. Proc. Seventh Solid Freeform Fabrication (SFF) Symposium, August 1996, Austin, Texas. pp. 307-312.

[15] A. Gupta, A.A. Ogale. Dual curing of carbon fiber reinforced photoresins for rapid prototyping. Polymer Composites, 23:6 (2002) 1162-1170.

[16] G. Zak, M.N. Sela, C.B. Park and B. Benhabib. A Layered-Manufacturing Process for the Fabrication of Glass Fiber-Reinforced Composites. Proc. Eighth Solid Freeform Fabrication (SFF) Symposium, August 1997, Austin, Texas, pp. 17-24.

[17] G. Zak, M. N. Sela, V. Yevko, C. B. Park, B. Benhabib. Layered-Manufacturing of Fiber-Reinforced Composites. J. Manuf. Sci. Eng, 121:3 (1999) 448-456.

[18] G. Zak, M. Haberer, C.B. Park, B. Benhabib, Mechanical properties of short-fibre layered composites: prediction and experiment. Rapid Prototyping Journal, 6:2 (2000) 107-118.

[19] D.E. Karalekas. Study of the mechanical properties of nonwoven fibre mat reinforced photopolymers used in rapid prototyping. Materials and Design, 24 (2003) 665-670.

[20] D. Klosterman, R. Chartoff, G. Graves, N. Osborne, B Priore. Interfacial characteristics of composites fabricated by laminated object manufacturing. Composites Part A, 29A (1998) 1165-1174.

[21] R. Bogue. 3D printing: the dawn of a new era in manufacturing? Assembly Automation, 33:4 (2013) 307-311.

[22] H. Prüß, T. Vietor. Design for Fiber-Reinforced Additive Manufacturing. Journal of Mechanical Design, 137:11 (2015), 111409.

[23] N. Mohan, P. Senthil, S. Vinodh, N. Jayanth. A review on composite materials and process parameters optimisation for the fused deposition modelling process. Virtual and Physical Prototyping, 12:1 (2017) 47-59.

[24] K. Croft, L. Lessard, D. Pasini, M. Hojjati, J. Chen, A. Yousefpour. Experimental study of the effect of automated fiber placement induced defects on performance of composite laminates. Composites: Part A 42 (2011) 484-491.

[25] B.T. Åstrom, R.B. Pipes. Thermoplastic Filament Winding with On-Line Impregnation. Journal of Thermoplastic Composite Materials, 3:4 (1990) 314-324.

[26] F. Henninger, K. Friedrich. Thermoplastic filament winding with online-impregnation. Part A: process technology and operating efficiency. Composites: Part A 33 (2002) 1479-1486.

[27] J.P. Nunes, J.F. Silva, P.J. Novo. Processing Thermoplastic Matrix Towpregs by Pultrusion. Advances in Polymer Technology, 32 (2012) E306-E312.

[28] F. Ning, W. Cong, J. Qiu, J. Wei, S. Wang. Additive manufacturing of carbon fiber reinforced thermoplastic composites using fused deposition modeling. Composites Part B, 80 (2015) 369-378.

[29] N. Li, Y. Li, S. Liu. Rapid prototyping of continuous carbon fiber reinforced polylactic acid composites by 3D printing. Journal of Materials Processing Technology, 238 (2016) 218-225.

[30] X. Tian, T. Liu, C. Yang, Q. Wang, D. Li. Interface and performance of 3D printed continuous carbon fiber reinforced PLA composites, Composites: Part A, 88 (2016) 198-205.

[31] G.W. Melenka, B.K.O. Cheung, J.S. Schofield, M.R. Dawson, J.P. Carey. Evaluation and prediction of the tensile properties of continuous fiber-reinforced 3D printed structures. Composite Structures, 153 (2016) 866-875.

[32] https://markforged.com (accessed June 28, 2016).

[33] ASTM D3039. Standard Test Method for Tensile Properties of Fiber-Resin Composites, ASTM International, West Conshohocken, PA, 2014.

[34] ASTM D695-02a. Standard Test Method for Compressive Properties of Rigid Plastics, ASTM International, West Conshohocken, PA, 2003.

[35] ASTM D3518. Standard Test Method for In-Plane Shear Response of Polymer Matrix Composite Materials by Tensile Test of a $\pm 45^{\circ}$ Laminate, ASTM International, West Conshohocken, PA, 2013.

[36] G. Promis, T.Q. Bach, A. Gabor, P. Hamelin. Failure behavior of E-glass fiber- and fabric-reinforced IPC composites under tension and compression loading. Materials and Structures, 47 (2014) 631-645.

[37] E. Correa, V. Mantič, F. París. A micromechanical view of inter-fibre failure of composite materials under compression transverse to the fibres, Composites Science and Technology 68:9 (2008) 2010-2021.

[38] https://www.acpsales.com/upload/Mechanical-Properties-of-Carbon-Fiber-Composite-Materials.pdf (accessed April 14, 2017).